

Fast and Accurate Gigapixel Pathological Image Classification with Hierarchical Distillation Multi-Instance Learning

Jiuyang Dong¹, Junjun Jiang^{1*}, Kui Jiang¹, Jiahao Li¹,
Yongbing Zhang^{2*}

¹Harbin Institute of Technology, ²Harbin Institute of Technology, Shenzhen

{jiuyang.dong, jiahao.li}@stu.hit.edu.cn,

{jiangjunjun, jiangkui, ybzhang08}@hit.edu.cn

Abstract

Although multi-instance learning (MIL) has succeeded in pathological image classification, it faces the challenge of high inference costs due to processing numerous patches from gigapixel whole slide images (WSIs). To address this, we propose HDMIL, a hierarchical distillation multi-instance learning framework that achieves fast and accurate classification by eliminating irrelevant patches. HDMIL consists of two key components: the dynamic multi-instance network (DMIN) and the lightweight instance pre-screening network (LIPN). DMIN operates on high-resolution WSIs, while LIPN operates on the corresponding low-resolution counterparts. During training, DMIN are trained for WSI classification while generating attention-score-based masks that indicate irrelevant patches. These masks then guide the training of LIPN to predict the relevance of each low-resolution patch. During testing, LIPN first determines the useful regions within low-resolution WSIs, which indirectly enables us to eliminate irrelevant regions in high-resolution WSIs, thereby reducing inference time without causing performance degradation. In addition, we further design the first Chebyshev-polynomials-based Kolmogorov-Arnold classifier in computational pathology, which enhances the performance of HDMIL through learnable activation layers. Extensive experiments on three public datasets demonstrate that HDMIL outperforms previous state-of-the-art methods, e.g., achieving improvements of 3.13% in AUC while reducing inference time by 28.6% on the Camelyon16 dataset. The project is available at <https://github.com/JiuyangDong/HDMIL>.

1. Introduction

Recently, multi-instance learning (MIL) has emerged as the leading approach for analyzing pathological whole slide

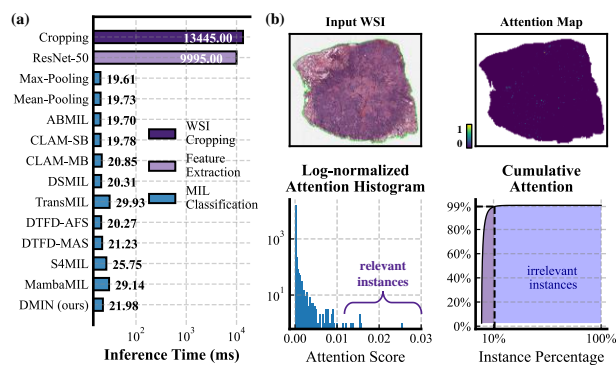


Figure 1. **What makes inference slow?** (a) **Time-consuming data pre-processing:** After comparing the time required for data pre-processing (WSI cropping, feature extraction) and MIL network classification, it is clear that data pre-processing is the main speed bottleneck. (b) **Redundant irrelevant patches:** For example, in a randomly selected WSI, numerous instances have extremely low attention scores [19], indicating their minimal contribution, if any, to the bag-level classification.

images (WSIs), demonstrating significant success in tasks such as tumor detection, subtyping [10, 27, 34, 41, 47, 61], tissue micro-environment quantification [13, 20, 35, 38, 44, 45], and survival prediction [6, 46, 57, 59].

To handle gigapixel WSIs, the MIL framework treats each WSI as a bag, cropping it into thousands of patches, each treated as an instance. Before being fed into the MIL networks for classification, all patches need to undergo feature extraction. Considering that each WSI contains thousands of patches, the process of WSI cropping and feature extraction can be very time-consuming. As shown in Fig. 1, data pre-processing is the primary speed bottleneck, requiring hundreds of times more time than the MIL classifiers. Moreover, WSIs often contain redundant patches with minimal contribution to the bag-level classification. For example, by adding up the attention scores of only a small frac-

*Corresponding author: Junjun Jiang, Yongbing Zhang

tion (about 10%) of the patches in the selected WSI, we can obtain 99% of the total attention scores. Therefore, the remaining patches can be safely considered as irrelevant and removed without affecting the performance.

Based on the above analysis, a straightforward idea to reduce the inference time is discarding irrelevant instances based on attention scores. Unfortunately, existing MIL algorithms need to extract the features of all cropped patches before calculating their attention scores, which brings up the “chicken and egg” problem. To accelerate WSI classification, Yu et al. proposed SMT [60]. Instead of cropping each WSI into patches, SMT employs cascading vision transformer (ViT) blocks to gradually search for “suspicious” areas and ultimately uses only a small area of the entire WSI for classification. As pointed out by Yu et al., the classification performance of SMT heavily relies on accurately identifying potential tumor areas. However, the pathological information provided by the low-resolution thumbnails, used as the initial input of SMT, is insufficient, which can easily lead to inappropriate regions of interest being focused. Consequently, the accumulation of errors results in inferior classification performance of SMT when compared to other non-accelerated MIL methods.

In this paper, we propose a hierarchical distillation multi-instance learning (HDMIL) framework aiming to quickly identify irrelevant patches and thus achieve fast and accurate classification. During training, instance-level features extracted from all cropped patches in the high-resolution WSIs are leveraged to train a dynamic multi-instance network (DMIN) with a self-distillation strategy. This self-distillation strategy constrains the teacher and student branches in DMIN, which use **all** and **partial** instances for classification respectively, to obtain consistent results, thus making the student branch selected instances non-irrelevant. Afterwards, we can obtain a binary mask for each instance depending on whether the instance is considered relevant to the slide classification. The masks are then utilized to guide the training of a lightweight instance pre-screening network (LIPN), which learns to identify the binary relevance of each patches in the corresponding low-resolution WSIs. During testing, after LIPN indicates irrelevant low-resolution patches, we can determine which high-resolution patches can be skipped, thereby saving inference time. Furthermore, a Chebyshev-polynomials-based Kolmogorov-Arnold (CKA) classifier is designed for more accurate classification, where learnable activation layers have powerful capabilities.

Overall, this paper makes three key contributions:

- This paper offers a crucial insight: eliminating irrelevant instances not only speeds up the inference process but also improves the classification performance. This finding challenges the conventional trade-off between speed and performance and provides valuable inspiration for fu-

ture research in multi-instance classification.

- We are the first to propose and apply the Chebyshev-polynomials-based Kolmogorov-Arnold classifier to computational pathology, which can greatly improve the classification performance.
- Extensive experiments on three public datasets demonstrate the effectiveness of our method. For example, on the Camelyon16 dataset, HDMIL achieves an AUC of 90.88% and an accuracy of 88.61%, outperforming previous best methods by 3.13% and 3.18%, respectively. Moreover, the inference time was reduced by 28.6%.

2. Related Work

MIL for WSI Classification. MIL for WSI classification can be divided into two categories: instance-based and embedding-based. Instance-based methods [9, 21, 24, 36, 39, 42, 63] first classify each instance and then aggregate the predictions using Max-Pooling, Mean-Pooling, or other pre-defined pooling operations to generate the final bag-level prediction. Embedding-based methods [10, 19, 27, 34, 47, 57, 61] use networks to assess the significance of each instance and weight all instances accordingly, producing the bag-level representation for classification. For the embedding-based methods, it is observed that different instances within each WSI have varying contributions to the bag-level representation. Building on this observation, we design the HDMIL framework to achieve fast and accurate classification by selectively removing irrelevant instances.

Dynamic Neural Networks. Dynamic neural networks [4, 14–18, 28, 30, 51, 56] can adjust their architecture dynamically according to the input data, thereby controlling the computational redundancy adaptively. In the era of Visual Transformers, many studies [31, 37, 43, 48, 53, 62] have attempted to improve inference efficiency by reducing token redundancy. In addition to bridging the gap in the field of computational pathology by utilizing dynamic networks to reduce instances and speed up inference, our HDMIL also addresses the aforementioned “chicken or egg” problem. This problem cannot be resolved using existing dynamic networks that solely rely on end-to-end training.

Kolmogorov-Arnold Networks. Most previous studies [8, 23, 25, 26, 32, 49] before KAN [33] used the original 2-layer structure to explore the possibility of constructing neural networks based on the Kolmogorov-Arnold representation theorem. KAN extended this theorem to networks of arbitrary width and depth, exploring its potential as a fundamental model of “AI+Science”. Subsequent research has primarily focused on improving the integration of KAN into various tasks [11, 12, 22, 29, 52, 54] or modify its architecture [1, 3, 5, 50, 55, 58]. In this paper, we propose to replace the spline function in KAN with first-kind Chebyshev polynomials to develop a more powerful MIL classifier for real-world pathological image classification.

3. Method

As illustrated in Fig. 2, our proposed HDMIL framework mainly consists of two stages: training and inference. As shown in Fig. 2(a), in the training stage, we first employ a **self-distillation training** strategy to train the DMIN on high-resolution WSIs for bag-level classification and indicating irrelevant regions. With the guidance from the trained DMIN, we perform **cross-distillation training** to get LIPN using low-resolution WSIs, which achieves discrimination of the binary importance (important or not) of each region with extremely low computational cost. In the inference stage, as shown in Fig. 2(b), LIPN relies on low-resolution WSIs to quickly identify regions that are irrelevant to classification and discard the corresponding patches within high-resolution WSIs. Subsequently, the remaining patches are fed into the feature extractor and DMIN to generate the classification results.

Before training, we first pre-process the input data following the standard procedure for pathological WSIs [34]. The dataset $\{X_i\}_{i=1}^S$ comprises S WSI pyramids with slide labels, where each X_i contains a pair of high-resolution ($20\times$) and low-resolution ($1.25\times$) WSIs, respectively referred to as $X_{i,HR}$ and $X_{i,LR}$. It should be noted that WSI pyramids typically contain WSIs at various magnification levels ranging from $1.25\times$ to $40\times$, but in this paper only the two representative magnifications are utilized. After removing the background regions, we get N_i pairs of 16×16 patches from $X_{i,LR}$ and 256×256 patches from $X_{i,HR}$.

3.1. Self-Distillation Training of DMIN

As shown in Fig. 2(c), DMIN is designed to classify high-resolution WSIs and identify instances irrelevant to the bag-level classification. Specifically, DMIN comprises five modules, namely, the projection module, attention module, teacher branch, student branch, and CKA classifiers.

Projection and Attention Module. During training, all patches extracted from the high-resolution WSI $X_{i,HR}$ are fed into a pre-trained feature extractor to generate a set of instance-level features $I_{i,HR}$. Subsequently, $I_{i,HR}$ is fed into the projection module for dimensionality reduction, producing a new feature set $F_{i,HR} \in \mathbb{R}^{N_i \times Q}$, where Q denotes the dimensionality of the reduced features. Then, the dimension-reduced $F_{i,HR}$ is fed into the attention module to compute the un-normalized attention scores:

$$A_{i,HR} = [\phi(F_{i,HR}V) \odot \sigma(F_{i,HR}U)]W, \quad (1)$$

where $\phi(\cdot)$ and $\sigma(\cdot)$ denote the tanh and sigmoid function. The weight matrices U , V , and W are the learnable parameters. The attention module here uses the same dual branch attention network as CLAM [34]. In the binary classification tasks discussed in this paper, the attention matrices corresponding to the first and second categories are denoted as $A_{i,HR,1} \in \mathbb{R}^{N_i \times 1}$ and $A_{i,HR,2} \in \mathbb{R}^{N_i \times 1}$, respectively.

Teacher Branch. The dimension-reduced $F_{i,HR}$ is then linearly weighted by the attention matrix for each category to produce the bag-level representation, which are used for final classification:

$$E_{i,HR,c}^{tea} = \varphi(A_{i,HR,c})^\top \otimes F_{i,HR,c}, c \in \{1, 2\}. \quad (2)$$

Here $\varphi(\cdot)$ represents the softmax function and $E_{i,HR,c}^{tea} \in \mathbb{R}^{1 \times Q}$ denotes the bag-level representation corresponding to the c -th category in the teacher branch.

Student Branch and Self-Distillation. The student branch is designed to compute bag-level representations using only a **subset** of instances with larger attention scores, and we impose a constraint to ensure that the bag-level representations in the student branch remain as consistent as possible with the representations obtained in the teacher branch using **all** the instances. In this way, the attention module is encouraged to focus more on instances that are important for bag-level classification and filters out irrelevant instances.

However, directly using instances with high attention scores is a discrete operation, resulting in a non-differentiable problem during optimization. To address this issue, we employ the Gumbel trick [43] to selectively choose instances with higher attention scores for end-to-end training. First, we incorporate the Gumbel Noise [18] to ‘‘sigmoid’’ the un-normalized attention matrices:

$$\hat{A}_{i,HR,c} = \sigma\left(\frac{A_{i,HR,c} + G_{1,c} - G_{2,c}}{\tau}\right), c \in \{1, 2\}. \quad (3)$$

Here σ represents the sigmoid function, $G_{1,c} \in \mathbb{R}^{N_i \times 1}$ and $G_{2,c} \in \mathbb{R}^{N_i \times 1}$ are two noises matrices randomly sampled from the Gumbel distribution, and τ is the temperature coefficient. Next, we binarize the ‘‘sigmoided’’ attention scores in a differentiable way:

$$M_{i,HR,c}^j = B(\hat{A}_{i,HR,c}^j, \gamma) - D(\hat{A}_{i,HR,c}^j) + \hat{A}_{i,HR,c}^j, \quad (4)$$

where $M_{i,HR,c}^j \in \{0, 1\}$ represents the mask value of the j -th instance and γ denotes the threshold as a hyperparameter. $B(a, b)$ here represents the discrete binarization function, which equals 1 when a is greater than b , and 0 otherwise. $D(\cdot)$ represents the gradient truncation operation.

Furthermore, we propose an **attention masking** mechanism to eliminate the impact of instances with zero mask values on the bag-level representations:

$$E_{i,HR,c}^{stu} = \sum_{j=1}^{N_i} \frac{\exp(A_{i,HR,c}^j) M_{i,HR,c}^j}{\sum_{s=1}^{N_i} \exp(A_{i,HR,c}^s) M_{i,HR,c}^s} F_{i,HR,c}^j, \quad (5)$$

where $E_{i,HR,c}^{stu} \in \mathbb{R}^{1 \times Q}$ represents the bag-level representation of the c -th class in the student branch.

CKA Classifier. In order to enhance the capacity of the MIL classifier, we propose to use the Kolmogorov-Arnold

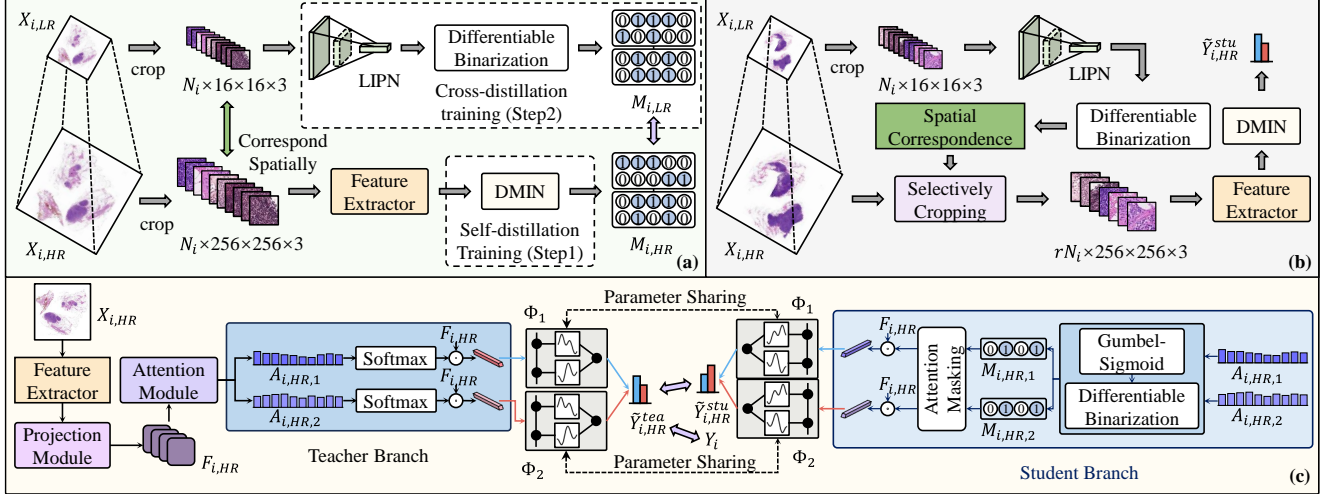


Figure 2. Overview of our **HDMIL** framework. (a) During training, we start by utilize the high-resolution WSI $X_{i,HR}$ for self-distillation of DMIN, enabling it to classify $X_{i,HR}$ and generate per-instance mask $M_{i,HR}$ which indicates the relevance of each region to the bag-level classification. Afterwards we froze DMIN and employ the masks $M_{i,HR}$ to distill LIPN, which learns the contribution of each region using the low-resolution $X_{i,LR}$. (b) During inference, the LIPN can identify which patches within $X_{i,HR}$ need to be used for classification by evaluating $X_{i,LR}$. (c) The self-distillation training of DMIN on the high-resolution $X_{i,HR}$.

network to learn nonlinear activation functions instead of using fixed activation functions in the classifier. Specifically, we employ the iterative form of K -order Chebyshev polynomials to represents the basis functions $T_K(x)$:

$$T_K(x) = 2xT_{K-1}(x) - T_{K-2}(x), K \geq 2. \quad (6)$$

Here $x \in \mathbb{R}^{1 \times Q}$ represents a bag-level representation, where the baseline condition are $T_0(x) = \mathbf{1}$ and $T_1(x) = x$. By multiplying the basis functions $T(x)$ by the learnable coefficients $\Omega \in \mathbb{R}^{Q \times O \times (K+1)}$, we can get the prediction of the classifier $\Phi(x)$:

$$\Phi(x)[o] = \sum_{k=0}^K \sum_{q=1}^Q T_k(x)[q] * \Omega[q, o, k], \quad (7)$$

where O represents the dimension of the prediction result. Since we use a dual-branch attention module, it's natural to calculate the classification results for the two branches individually, so O is equal to 1, and the predictions of the teacher branch and the student branch are:

$$\begin{cases} \tilde{Y}_{i,HR}^{tea} = [\Phi_1(\phi(E_{i,HR,1}^{tea})) \oplus \Phi_2(\phi(E_{i,HR,2}^{tea}))], \\ \tilde{Y}_{i,HR}^{stu} = [\Phi_1(\phi(E_{i,HR,1}^{stu})) \oplus \Phi_2(\phi(E_{i,HR,2}^{stu}))]. \end{cases} \quad (8)$$

Here \oplus represents the concatenation operation and the tanh function ϕ maps the input values of the CKA classifiers to $[-1, 1]$, ensuring that the inputs meet the requirements of the Chebyshev polynomial.

Hybrid Loss Function. The training objectives of DMIN are threefolds: 1) The teacher branch can correctly classify $X_{i,HR}$; 2) The classification results of the student

branch (using partial instances) and teacher branch (using all instances) should be consistent; 3) The proportion of instances selected should be controllable. Specifically, we first use the cross-entropy loss L_{cls}^{tea} to ensure that the teacher branch performs accurate classification:

$$L_{cls}^{tea} = CE(\tilde{Y}_{i,HR}^{tea}, Y_i), \quad (9)$$

where $CE(\cdot)$ represents the cross entropy loss function and Y_i is the slide-level label of X_i . Next, we constrain the bag-level representation $E_{i,HR}^{stu}$ and classification logit $\tilde{Y}_{i,HR}^{stu}$ in the student branch by knowledge distillation:

$$\begin{cases} L_{dis,1}^{stu} = L_2(E_{i,HR}^{stu}, E_{i,HR}^{tea}), \\ L_{dis,2}^{stu} = L_{KL}(\tilde{Y}_{i,HR}^{stu}, \tilde{Y}_{i,HR}^{tea}). \end{cases} \quad (10)$$

Here, $L_2(\cdot)$ and $L_{KL}(\cdot)$ denote the 2-norm and KL divergence loss function, respectively. Finally, we constrain the proportion of learned relevant instances $\tilde{r}_{i,HR}$ to be close to a preset retention ratio r :

$$L_{rate}^{stu} = L_2(\tilde{r}_{i,HR}, r). \quad (11)$$

Here, the j -th instance is considered relevant if either $M_{i,HR,1}^j$ or $M_{i,HR,2}^j$ are not zero. Additionally, we utilize the clustering loss L_{clu}^{tea} proposed in CLAM [34] to optimize the feature space of DMIN. In conclusion, the hybrid loss function of DMIN is:

$$L_{DMIN} = \alpha_1 L_{cls}^{tea} + \alpha_2 L_{clu}^{tea} + \alpha_3 L_{dis,1}^{stu} + \alpha_4 L_{dis,2}^{stu} + \alpha_5 L_{rate}^{stu}. \quad (12)$$

For the coefficients of different loss terms, we did not perform hyper-parameter search, but empirically set α_1 and α_2 to 0.7 and 0.3 according to CLAM [34], and set α_3 , α_4 , and α_5 to 0.5, 0.5, and 2.0 according to DynamicViT [43].

3.2. Cross-Distillation Training of LIPN

Although DMIN can successfully identify irrelevant regions within WSIs, it does not improve the inference speed. This is because DMIN needs to use all patches’ features generated by the feature extractor to determine which instances should be discarded. However, this patch-wise feature extraction is actually the bottleneck for WSI inference speed. To solve this problem, we propose using DMIN to distill LIPN, a lightweight instance pre-screening network specifically tailored for low-resolution WSIs, as shown in Fig. 2(a). After training, LIPN can quickly identify the irrelevant regions within low-resolution WSIs, thereby indirectly indicating the irrelevant patches within high-resolution WSIs.

Specifically, the N_i 16×16 patches obtained from $X_{i,LR}$ are directly fed into LIPN, generating dual-branch prediction matrices $P_{i,LR,c}, c \in \{1, 2\}$ for the two categories. Since these low-resolution patches contain relatively little information, we do not require LIPN to learn the specific contribution score of each patch to the bag-level classification like DMIN does. On the contrary, it is easier for LIPN to learn whether each patch contributes to the bag-level classification or not. Therefore, $P_{i,LR,c}$ is first binarized:

$$M_{i,LR,c}^j = B(P_{i,LR,c}^j, \gamma) - D(P_{i,LR,c}^j) + P_{i,LR,c}^j. \quad (13)$$

Next, $M_{i,LR,c}$ is forced to be consistent with $M_{i,HR,c}$, so that $M_{i,LR,c}$ can also indicate whether a patch is relevant. What’s more, the ratio of learned relevant patches $\tilde{r}_{i,LR}$ is also constrained to be close to r . Overall, the hybrid loss function of LIPN is:

$$L_{LIPN} = \beta_1 \sum_{c=1}^2 \frac{L_1(M_{i,LR,c}, M_{i,HR,c})}{2} + \beta_2 L_2(\tilde{r}_{i,LR}, r). \quad (14)$$

Here, $L_1(\cdot)$ denotes the 1-norm loss function. In our implementation, we employed the widely-used ResNet-50 pre-trained on ImageNet as the feature extractor, and used a lightweight variant of MobileNetV4 [40] for the pre-screening network LIPN. The detailed architecture of LIPN is illustrated in the supplementary material.

3.3. Efficient Inference

As shown in Fig. 2(b), our proposed efficient inference process consists of three steps: 1) Cropping all patches from $X_{i,LR}$, with the total number of patches being N_i . 2) Feeding these patches into LIPN to identify regions relevant to classification, generating $M_{i,LR}$; 3) Selectively cropping relevant $\tilde{r}_{i,LR}N_i$ patches from $X_{i,HR}$ based on $M_{i,LR}$, and

then feeding them into the feature extractor and DMIN. Afterwards, we calculate the bag-level representations and the final classification results using the student branch across categories separately.

4. Experimental Results

4.1. Settings

We evaluated our proposed algorithm on three public datasets: 1) for breast cancer lymph node metastasis detection using the Camelyon16 [2] dataset; 2) for lung cancer subtyping using the TCGA-NSCLC dataset; and 3) for breast cancer subtyping using the TCGA-BRCA dataset. All WSIs were pre-processed using tools developed by CLAM [34]. All experiments adhered to the principle of **10-fold Monte Carlo cross-validation**. For Camelyon16, the official training set was divided into training and validation sets at a 9:1 ratio based on the number of cases in each fold, while the official test set was used for testing across all folds. The TCGA-NSCLC and TCGA-BRCA datasets were split into the training, validation, and test sets in an 8:1:1 ratio, again based on the number of cases in each fold. The implementation details are in the supplementary material.

4.2. Comparative Results on Test Sets

Classification Performance. Table 1 compares the classification performance of our proposed HDMIL against existing MIL methods on the Camelyon16 [2], TCGA-NSCLC, and TCGA-BRCA test sets. HDMIL \dagger means using only DMIN for inference without pre-screening instances through LIPN. From the table we can find: 1) Both HDMIL \dagger and HDMIL consistently outperform existing methods across these datasets. 2) When the dataset is large enough, the speedup brought by HDMIL does not mean a decrease in classification performance. For example, the test performance gap between HDMIL \dagger and HDMIL is small on TCGA-NSCLC and TCGA-BRCA, both of which contain about 1000 WSIs. Meanwhile, the AUC score of HDMIL decreases slightly on Camelyon16, but is still much better than existing MIL methods. We believe that the performance degradation of HDMIL compared to HDMIL \dagger on the Camelyon16 dataset can be primarily attributed to the small dataset size (less than 400 WSIs), rather than inherent shortcomings of HDMIL itself. A further analysis is presented in Sec. 4.5.

Inference Time. From Tab. 1, it is evident that the processing time of HDMIL \dagger is nearly identical to that of existing methods since they need to **process the same number of high-resolution patches**. However, HDMIL outperforms all other methods, significantly reducing the processing time. Compared to HDMIL \dagger , HDMIL achieves a total speed improvement of 28.6%, 21.8%, and 7.2% on the three datasets, respectively. To analyze how HDMIL

Comparative Methods	Camelyon16			TCGA-NSCLC			TCGA-BRCA		
	AUC \uparrow	ACC \uparrow	Time(s) \downarrow	AUC \uparrow	ACC \uparrow	Time(s) \downarrow	AUC \uparrow	ACC \uparrow	Time(s) \downarrow
Max-Pooling	83.26 _{1.54}	82.41 _{0.73}	23.46	94.66 _{2.33}	86.40 _{3.73}	57.16	88.03 _{7.76}	86.05 _{3.88}	36.49
Mean-Pooling	61.80 _{2.15}	70.54 _{1.41}	23.46	92.82 _{3.54}	84.93 _{4.78}	57.16	88.23 _{5.67}	86.74 _{2.44}	36.49
ABMIL [19]	84.88 _{3.38}	82.79 _{2.68}	23.46	94.92 _{2.29}	88.03 _{3.65}	57.16	87.70 _{6.15}	87.68 _{3.51}	36.49
CLAMSB [34]	83.49 _{4.46}	79.61 _{4.40}	23.46	95.05 _{2.72}	88.74 _{3.39}	57.16	88.25 _{6.12}	87.58 _{4.92}	36.49
CLAMMB [34]	87.51 _{3.23}	82.56 _{3.11}	23.46	95.59 _{2.16}	88.01 _{3.38}	57.16	90.22 _{5.18}	88.27 _{3.52}	36.49
DSMIL [27]	75.94 _{10.81}	75.35 _{6.12}	23.46	92.11 _{2.97}	83.67 _{3.80}	57.16	83.33 _{7.48}	82.59 _{3.66}	36.49
TransMIL [47]	82.26 _{5.67}	81.01 _{6.85}	23.47	94.57 _{2.03}	88.21 _{3.04}	57.17	88.33 _{5.73}	87.55 _{3.78}	36.49
DTFDAFS [61]	87.40 _{3.17}	85.12 _{2.42}	23.46	95.59 _{2.08}	88.76 _{3.89}	57.16	87.24 _{7.38}	86.83 _{3.98}	36.49
DTFDMAS [61]	87.75 _{2.07}	85.43 _{2.03}	23.46	95.02 _{2.32}	89.02 _{3.78}	57.17	87.80 _{9.65}	87.48 _{4.13}	36.49
S4MIL [10]	86.40 _{1.99}	80.39 _{2.79}	23.47	96.19 _{1.89}	89.69 _{2.86}	57.17	90.40 _{5.73}	88.17 _{3.88}	36.49
MambaMIL [57]	87.06 _{6.19}	83.26 _{2.93}	23.47	95.37 _{1.70}	89.62 _{3.13}	57.16	89.69 _{5.91}	87.78 _{4.27}	36.49
HDMIL \dagger	93.17 _{1.83}	88.92 _{2.51}	23.46	96.47 _{2.20}	89.75 _{2.86}	57.16	90.43 _{4.86}	88.68 _{3.17}	36.49
HDMIL	90.88 _{2.75}	88.61 _{2.04}	16.75	96.35 _{2.26}	89.78 _{3.11}	44.71	90.45 _{4.42}	88.27 _{2.47}	33.86

Table 1. Comparison of HDMIL with the state-of-the-art MIL methods on Camelyon16, TCGA-NSCLC, and TCGA-BRCA. The 10-fold test AUC and accuracy (ACC) scores are reported in the form of mean_{std}. The best and second best results are indicated in red and blue, respectively. The average processing time per WSI on each test sets are also shown. HDMIL \dagger means using only DMIN for inference.

Methods	Dataset	LIPN	Crop	Fea	DMIN	Total
Came16	HDMIL \dagger	-	13.45	10.00	0.02	23.46
	HDMIL	0.01	10.88	5.84	0.02	16.75
	Δ	-	-19.1%	-41.6%	-	-28.6%
NSCLC	HDMIL \dagger	-	47.02	10.12	0.02	57.16
	HDMIL	0.01	37.21	7.48	0.02	44.71
	Δ	-	-20.9%	-26.1%	-	-21.8%
BRCA	HDMIL \dagger	-	27.17	9.30	0.02	36.49
	HDMIL	0.01	25.84	8.00	0.02	33.86
	Δ	-	-4.90%	-14.0%	-	-7.2%

Table 2. Comparison of HDMIL and HDMIL \dagger when splitting the inference time (seconds) into four stages: instance pre-screening (LIPN), WSI cropping (“Crop”), feature extraction (“Fea”), and bag classification (DMIN).

achieves this time-saving effect, we divide the WSI inference process into four stages: instance pre-screening, WSI cropping, feature extraction, and MIL classification, as presented in Tab. 2. Although LIPN causes a slight increase in inference time (approximately 0.01 seconds), it reduces the number of instances that require cropping and feature extraction, thereby significantly reducing total inference time.

4.3. Focusing and Discarding Visualization

Figure 3 shows two tumor WSIs with patch-level annotations, attention maps generated by DMIN, the instance retention after LIPN pre-screening, DMIN-focused patches, and LIPN-discarded patches. As expected, the first branch of DMIN focuses on normal tissue regions, while the second branch emphasizes tumor regions, demonstrating

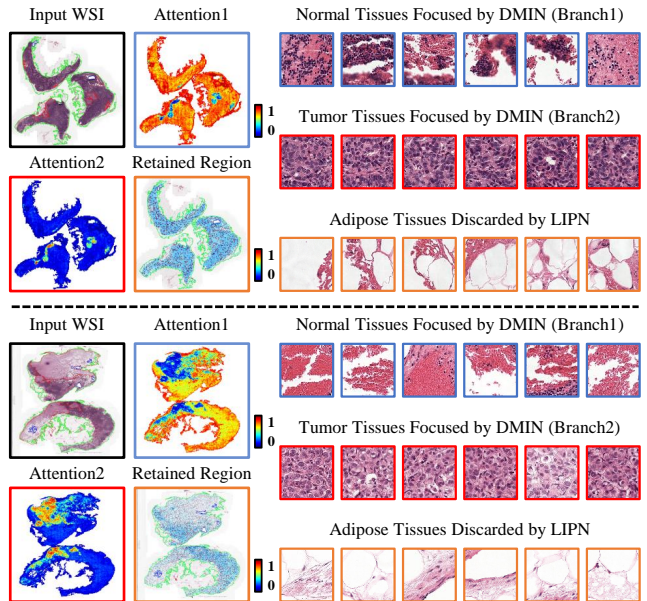


Figure 3. Visualization analysis of two randomly selected WSIs. The pathologists marked the tumor areas in the input WSIs with red lines. The dual-branch attention maps in DMIN (“Attention1” and “Attention2”) are shown, and the instances selected by LIPN are marked with blue masks (“Retained Region”)

DMIN’s ability to identify regions related to bag-level classification. Moreover, the regions to which DMIN assigns greater importance are retained by LIPN, while instances derived from adipose tissues, which contribute minimally to classification, are effectively discarded by LIPN.

DMIN		LIPN	Camelyon16		TCGA-NSCLC		TCGA-BRCA		Average	
CKA	SelfDist		AUC	ACC	AUC	ACC	AUC	ACC	AUC	ACC
✗	✗	✗	94.67 _{4.51}	91.54 _{5.38}	95.36 _{3.51}	89.44 _{4.51}	88.82 _{6.41}	86.47 _{4.21}	92.95	89.15
✓	✗	✗	97.15 _{3.27}	93.85 _{4.86}	95.19 _{3.01}	89.67 _{3.57}	91.22 _{5.40}	89.00 _{3.62}	94.52	90.84
✓	✓	✗	97.70 _{2.54}	95.00 _{4.81}	95.58 _{3.27}	90.29 _{3.90}	93.33 _{4.58}	89.83 _{2.71}	95.54	91.71
✓	✓	✓	97.64 _{2.93}	95.38 _{3.97}	95.88 _{3.02}	90.50 _{3.44}	93.27 _{4.87}	88.70 _{3.92}	95.60	91.53

Table 3. The effect of each component in HDMIL on classification performance. The 10-fold **validation** AUC and ACC scores are reported in the form of mean_{std}. “SelfDist” is the abbreviation for self-distillation.

	Projection	Attention	Classifier
Params	7.082M	3.942M	0.828M
AUC	92.79 _{6.92}	85.03 _{8.36}	97.15 _{3.27}
ACC	86.54 _{9.11}	77.31 _{6.40}	93.85 _{4.86}

(1) Comparison of the position of the CKA layer.

	FC	MLP	KA [33]	CKA
Params	0.791M	1.842M	0.828M	0.828M
AUC	94.67 _{4.51}	94.97 _{5.05}	96.42 _{2.88}	97.15 _{3.27}
ACC	91.54 _{5.38}	92.69 _{6.13}	91.16 _{6.03}	93.85 _{4.86}

(2) Comparison of FC, MLP, KA, and CKA as classifiers.

	K=4	K=8	K=12	K=16
Params	0.803M	0.816M	0.828M	0.840M
AUC	94.67 _{4.29}	94.61 _{4.48}	97.15 _{3.27}	96.18 _{2.59}
ACC	89.62 _{7.91}	90.38 _{7.08}	93.85 _{4.86}	90.39 _{6.60}

(3) Comparison of using different orders in CKA classifier.

Table 4. Analysis of the CKA classifier. The 10-fold **validation** performance on the Camelyon16 dataset are reported.

4.4. Ablation Study on Validation Sets

Effect of Each Components. Table 3 presents the impact of each module in HDMIL on the classification results. Notably, replacing the conventional linear layer-based classifier with the proposed CKA classifiers and incorporating self-distillation into the DMIN training, both significantly improve the classification performance. In addition, using LIPN for instance pre-screening does not result in a obvious decrease in the classification performance on the validation set, slightly differing from the situation on the test set in Tab. 1. This will also be discussed in Sec. 4.5. In the following subsections, we analyze the reasons why each component works by 10-fold cross-validation experiments.

CKA Classifier in DMIN. As shown in Tab. 4, we analyze the proposed CKA classifiers from three perspectives: 1) the impact of employing the CKA layer at different positions; 2) comparison with other classification layers; and 3) the impact of different Chebyshev polynomial orders K . To

eliminate the impact of other factors, all experiments here only utilize the teacher branch trained on all instances.

- When using CKA layers as the projection or attention module, the number of trainable parameters increases dramatically, accompanied by a significant drop in performance. It seems that our CKA layer is also better at solving modeling problems in lower dimensional spaces, similar to the vanilla KAN [33].
- When compared with other classifiers such as the FC layer, two-layer MLP, and KA [33] layer, CKA demonstrates superior classification performance. Although FC, MLP, and KA can sometimes achieve similar performance to CKA in certain folds, there tends to be a larger performance gap in other folds. Thus, CKA is a more powerful and robust classifier.
- When the Chebyshev polynomial order changes from 4 to 16, the number of parameters of the entire DMIN does not change much. Nevertheless, there is a noticeable disparity in classification performance, with the best outcome achieved at an order of 12. Further increasing the order does not lead to better improvements in classification performance, probably due to the limited training data.

Self-Distillation of DMIN. We believe that self-distillation enhances the classification performance by enforcing the attention module to focus on crucial instances, thereby reducing the impact of irrelevant regions. This can be seen as a form of “denoising”. To verify this viewpoint, we evaluated the quality of the bags after the “denoising” effect of self-distillation by considering three types of instances to represent each bag: all instances within each WSI, instances selected by the trained DMIN, and randomly sampled instances. Newly trained Max-Pooling models are used to evaluate the quality of these three types of bags like linear probing [7]. As shown in Tab. 5, MIL models trained with instances selected by DMIN outperform models trained with randomly sampled instances and even outperform models trained with all instances. This suggests that self-distillation **improves the quality of bags** for classification by instance selection.

Distillation Methods in LIPN. Table 6 explores the effects of different distillation methods when using DMIN to distill LIPN. The symbol $A_H \rightarrow P_L$ represents the dis-

Metrics	All	Random	DMIN
AUC/ACC	92.06/84.62	89.40/83.46	92.73/85.78

Table 5. Average performance of Max-Pooling trained with different kinds of bags on the Camelyon16 **validation** set. The number of instances in each “random” bag were kept consistent with the number of instances in each “DMIN” bag.

tillation from attention $A_{i,HR}$ to instance-wise predictions $P_{i,LR}$, while $M_H \rightarrow M_L$ denotes the distillation between $M_{i,HR}$ and $M_{i,LR}$. It can be seen that distilling among discrete masks yields significantly better results, especially on the Camelyon16 dataset. This is because low-resolution patches lose too much information, in which case learning to predict the specific contribution score of each instance becomes challenging for LIPN, compared to learning the binary decision of the instance (keep or discard).

Distillation Manner	Camelyon16		TCGA-NSCLC		TCGA-BRCA	
	AUC	ACC	AUC	ACC	AUC	ACC
$A_H \rightarrow P_L$	81.70	83.85	95.01	89.29	90.49	87.10
$M_H \rightarrow M_L$	97.64	95.38	95.88	90.50	93.27	88.70

Table 6. Performance of HDMIL on the **validation** set when using different distillation methods. A_H , P_L , M_H , and M_L are the abbreviations for $A_{i,HR}$, $P_{i,LR}$, $M_{i,HR}$, and $M_{i,LR}$ respectively.

Impact of the Preset Instance Retention Ratio. We examine the impact of the preset instance ratio r on the classification performance, actual learned instance retention ratios, and inference time, as depicted in Fig. 4: 1) Generally, the performance of HDMIL and HDMIL \dagger exhibits a pattern of initial improvement followed by a decline as r increases. This can be attributed to the fact that when r is small, the scarcity of patches leads to the loss of classification-related information. Conversely, when r becomes excessively large, the self-distillation training fails to eliminate the interference caused by irrelevant instances. 2) In addition, it can be seen that the instance retention rate actually learned by HDMIL \dagger and HDMIL is roughly equivalent to the preset r . 3) The inference time gradually increases as r increases. When r reaches 0.9, the total inference time of HDMIL surpasses that of HDMIL \dagger due to the minimal number of discarded instances and the additional processing time for low-resolution WSIs.

4.5. Further Analysis: the Impact of Dataset Size

Despite the performance gap between HDMIL \dagger and HDMIL on the Camelyon16 test set (depicted in Tab. 1), both methods show similar performance on the validation sets across all three datasets (shown in Tab. 3 and Fig. 4). The drop in performance of HDMIL, on the Camelyon16 test

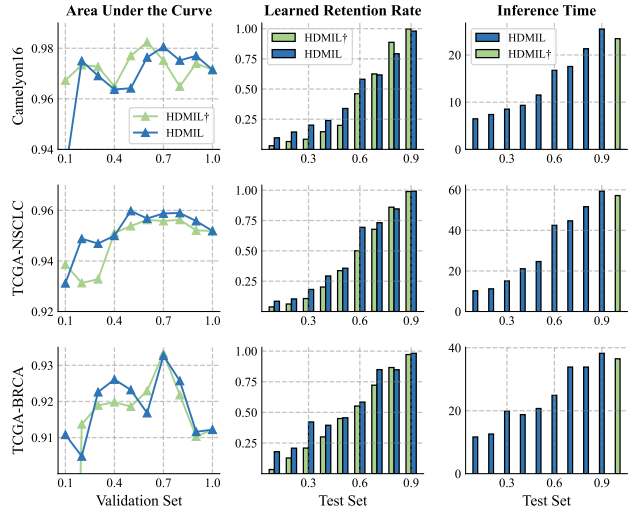


Figure 4. The impact of the preset instance retention rate r (hyperparameter) on classification performance, actual learned instance retention ratio, and inference time (seconds).

set, is likely attributed to the bias introduced by selecting models for evaluation based on their validation performance. This bias can result in suboptimal performance on the test sets, especially when there is a distribution difference between the validation and test sets, which becomes more pronounced when dealing with smaller datasets.

TCGA-NSCLC		TCGA-BRCA	
Valid Set	Test Set	Valid Set	Test Set
25% 100%	25% 100%	25% 100%	25% 100%
95.84 95.88	95.46 96.35	94.55 93.27	90.06 90.45

Table 7. The 10-fold average validation and test AUC scores of HDMIL, when the number of cases in the validation set is reduced to 25% and the cases in the training and test sets are unchanged.

To demonstrate our point, we conducted specific experiments on TCGA-NSCLC and TCGA-BRCA, as shown in Tab. 7. It can be found that when the number of cases in the validation set was reduced to 25% of the original size, the performance of HDMIL on the validation set did not decrease significantly, while the models selected using these validation sets performed worse on the test sets. This finding demonstrates that the performance decline of HDMIL on Camelyon16 can be attributed to the small dataset size rather than inherent algorithmic flaws.

5. Conclusion

In this paper, HDMIL offers a novel approach for accelerating WSI classification while ensuring high classification accuracy. By hierarchical-distillation, HDMIL efficiently

filters out irrelevant patches within WSIs, significantly reducing inference time. Extensive experiments demonstrate that HDMIL outperforms current state-of-the-art methods in both classification performance and inference speed. To further improve MIL efficiency, we will explore strategies to alleviate the inference burden on the feature extractor and integrate them with HDMIL in the future.

References

- [1] Alireza Afzal Aghaei. rkan: Rational kolmogorov-arnold networks. *arXiv preprint arXiv:2406.14495*, 2024. 2
- [2] Babak Ehteshami Bejnordi, Mitko Veta, Paul Johannes Van Diest, Bram Van Ginneken, Nico Karssemeijer, Geert Litjens, Jeroen AWM Van Der Laak, Meyke Hermesen, Quirine F Manson, Maschenka Balkenhol, et al. Diagnostic assessment of deep learning algorithms for detection of lymph node metastases in women with breast cancer. *Jama*, 318(22):2199–2210, 2017. 5
- [3] Alexander Dylan Bodner, Antonio Santiago Tepsich, Jack Natan Spolski, and Santiago Pourteau. Convolutional kolmogorov-arnold networks. *arXiv preprint arXiv:2406.13155*, 2024. 2
- [4] Tolga Bolukbasi, Joseph Wang, Ofer Dekel, and Venkatesh Saligrama. Adaptive neural networks for efficient inference. In *International Conference on Machine Learning*, pages 527–536. PMLR, 2017. 2
- [5] Zavareh Bozorgasl and Hao Chen. Wav-kan: Wavelet kolmogorov-arnold networks. *arXiv preprint arXiv:2405.12832*, 2024. 2
- [6] Richard J Chen, Ming Y Lu, Muhammad Shaban, Chengkuan Chen, Tiffany Y Chen, Drew FK Williamson, and Faisal Mahmood. Whole slide images are 2d point clouds: Context-aware survival prediction using patch-based graph convolutional networks. In *Medical Image Computing and Computer Assisted Intervention—MICCAI 2021: 24th International Conference, Strasbourg, France, September 27–October 1, 2021, Proceedings, Part VIII 24*, pages 339–349. Springer, 2021. 1
- [7] Ting Chen, Simon Kornblith, Mohammad Norouzi, and Geoffrey Hinton. A simple framework for contrastive learning of visual representations. In *International conference on machine learning*, pages 1597–1607. PMLR, 2020. 7
- [8] Daniele Fakhoury, Emanuele Fakhoury, and Hendrik Speleers. Exspline: An interpretable and expressive spline-based neural network. *Neural Networks*, 152:332–346, 2022. 2
- [9] Ji Feng and Zhi-Hua Zhou. Deep miml network. In *Proceedings of the AAAI conference on artificial intelligence*, 2017. 2
- [10] Leo Fillioux, Joseph Boyd, Maria Vakalopoulou, Paul-Henry Cournède, and Stergios Christodoulidis. Structured state space models for multiple instance learning in digital pathology. In *International Conference on Medical Image Computing and Computer-Assisted Intervention*, pages 594–604. Springer, 2023. 1, 2, 6
- [11] Remi Genet and Hugo Inzirillo. Tkan: Temporal kolmogorov-arnold networks. *arXiv preprint arXiv:2405.07344*, 2024. 2
- [12] Remi Genet and Hugo Inzirillo. A temporal kolmogorov-arnold transformer for time series forecasting. *arXiv preprint arXiv:2406.02486*, 2024. 2
- [13] Simon Graham, Quoc Dang Vu, Shan E Ahmed Raza, Ayesha Azam, Yee Wah Tsang, Jin Tae Kwak, and Nasir Rajpoot. Hover-net: Simultaneous segmentation and classification of nuclei in multi-tissue histology images. *Medical image analysis*, 58:101563, 2019. 1
- [14] Yizeng Han, Gao Huang, Shiji Song, Le Yang, Honghui Wang, and Yulin Wang. Dynamic neural networks: A survey. *IEEE Transactions on Pattern Analysis and Machine Intelligence*, 44(11):7436–7456, 2021. 2
- [15] Yizeng Han, Yifan Pu, Zihang Lai, Chaofei Wang, Shiji Song, Junfeng Cao, Wenhui Huang, Chao Deng, and Gao Huang. Learning to weight samples for dynamic early-exiting networks. In *European conference on computer vision*, pages 362–378. Springer, 2022.
- [16] Yizeng Han, Dongchen Han, Zeyu Liu, Yulin Wang, Xuran Pan, Yifan Pu, Chao Deng, Junlan Feng, Shiji Song, and Gao Huang. Dynamic perceiver for efficient visual recognition. In *Proceedings of the IEEE/CVF International Conference on Computer Vision*, pages 5992–6002, 2023.
- [17] Yizeng Han, Zeyu Liu, Zhihang Yuan, Yifan Pu, Chaofei Wang, Shiji Song, and Gao Huang. Latency-aware unified dynamic networks for efficient image recognition. *IEEE Transactions on Pattern Analysis and Machine Intelligence*, 2024.
- [18] Charles Herrmann, Richard Strong Bowen, and Ramin Zabih. Channel selection using gumbel softmax. In *European conference on computer vision*, pages 241–257. Springer, 2020. 2, 3
- [19] Maximilian Ilse, Jakub Tomczak, and Max Welling. Attention-based deep multiple instance learning. In *International conference on machine learning*, pages 2127–2136. PMLR, 2018. 1, 2, 6
- [20] Sajid Javed, Arif Mahmood, Muhammad Moazam Fraz, Navid Alemi Koohbanani, Ksenija Benes, Yee-Wah Tsang, Katherine Hewitt, David Epstein, David Snead, and Nasir Rajpoot. Cellular community detection for tissue phenotyping in colorectal cancer histology images. *Medical image analysis*, 63:101696, 2020. 1
- [21] James Keeler, David Rumelhart, and Wee Leow. Integrated segmentation and recognition of hand-printed numerals. *Advances in neural information processing systems*, 3, 1990. 2
- [22] William Knottenbelt, Zeyu Gao, Rebecca Wray, Woody Zhi-dong Zhang, Jiashuai Liu, and Mireia Crispin-Ortuzar. Coxkan: Kolmogorov-arnold networks for interpretable, high-performance survival analysis. *arXiv preprint arXiv:2409.04290*, 2024. 2
- [23] Mario Köppen. On the training of a kolmogorov network. In *Artificial Neural Networks—ICANN 2002: International Conference Madrid, Spain, August 28–30, 2002 Proceedings 12*, pages 474–479. Springer, 2002. 2

- [24] Oren Z Kraus, Jimmy Lei Ba, and Brendan J Frey. Classifying and segmenting microscopy images with deep multiple instance learning. *Bioinformatics*, 32(12):i52–i59, 2016. 2
- [25] Ming-Jun Lai and Zhaiming Shen. The kolmogorov superposition theorem can break the curse of dimensionality when approximating high dimensional functions. *arXiv preprint arXiv:2112.09963*, 2021. 2
- [26] Pierre-Emmanuel Leni, Yohan D Fougere, and Frédéric Truchetet. The kolmogorov spline network for image processing. In *Image Processing: Concepts, Methodologies, Tools, and Applications*, pages 54–78. IGI Global, 2013. 2
- [27] Bin Li, Yin Li, and Kevin W Eliceiri. Dual-stream multiple instance learning network for whole slide image classification with self-supervised contrastive learning. In *Proceedings of the IEEE/CVF conference on computer vision and pattern recognition*, pages 14318–14328, 2021. 1, 2, 6
- [28] Changlin Li, Guangrun Wang, Bing Wang, Xiaodan Liang, Zhihui Li, and Xiaojun Chang. Dynamic slimmable network. In *Proceedings of the IEEE/CVF Conference on computer vision and pattern recognition*, pages 8607–8617, 2021. 2
- [29] Chenxin Li, Xinyu Liu, Wuyang Li, Cheng Wang, Hengyu Liu, and Yixuan Yuan. U-kan makes strong backbone for medical image segmentation and generation. *arXiv preprint arXiv:2406.02918*, 2024. 2
- [30] Yanwei Li, Lin Song, Yukang Chen, Zeming Li, Xiangyu Zhang, Xingang Wang, and Jian Sun. Learning dynamic routing for semantic segmentation. In *Proceedings of the IEEE/CVF conference on computer vision and pattern recognition*, pages 8553–8562, 2020. 2
- [31] Youwei Liang, Chongjian Ge, Zhan Tong, Yibing Song, Jue Wang, and Pengtao Xie. Not all patches are what you need: Expediting vision transformers via token reorganizations. *arXiv preprint arXiv:2202.07800*, 2022. 2
- [32] Ji-Nan Lin and Rolf Unbehauen. On the realization of a kolmogorov network. *Neural Computation*, 5(1):18–20, 1993. 2
- [33] Ziming Liu, Yixuan Wang, Sachin Vaidya, Fabian Ruehle, James Halverson, Marin Soljačić, Thomas Y Hou, and Max Tegmark. Kan: Kolmogorov-arnold networks. *arXiv preprint arXiv:2404.19756*, 2024. 2, 7
- [34] Ming Y Lu, Drew FK Williamson, Tiffany Y Chen, Richard J Chen, Matteo Barbieri, and Faisal Mahmood. Data-efficient and weakly supervised computational pathology on whole-slide images. *Nature biomedical engineering*, 5(6):555–570, 2021. 1, 2, 3, 4, 5, 6
- [35] Faisal Mahmood, Daniel Borders, Richard J Chen, Gregory N McKay, Kevan J Salimian, Alexander Baras, and Nicholas J Durr. Deep adversarial training for multi-organ nuclei segmentation in histopathology images. *IEEE transactions on medical imaging*, 39(11):3257–3267, 2019. 1
- [36] Oded Maron and Tomás Lozano-Pérez. A framework for multiple-instance learning. *Advances in neural information processing systems*, 10, 1997. 2
- [37] Lingchen Meng, Hengduo Li, Bor-Chun Chen, Shiyi Lan, Zuxuan Wu, Yu-Gang Jiang, and Ser-Nam Lim. Adavit: Adaptive vision transformers for efficient image recognition. In *Proceedings of the IEEE/CVF Conference on Computer Vision and Pattern Recognition*, pages 12309–12318, 2022. 2
- [38] Erick Moen, Dylan Bannon, Takamasa Kudo, William Graf, Markus Covert, and David Van Valen. Deep learning for cellular image analysis. *Nature methods*, 16(12):1233–1246, 2019. 1
- [39] Pedro O Pinheiro and Ronan Collobert. From image-level to pixel-level labeling with convolutional networks. In *Proceedings of the IEEE conference on computer vision and pattern recognition*, pages 1713–1721, 2015. 2
- [40] Danfeng Qin, Chas Leichner, Manolis Delakis, Marco Fornoni, Shixin Luo, Fan Yang, Weijun Wang, Colby Banbury, Chengxi Ye, Berkin Akin, et al. Mobilenetv4-universal models for the mobile ecosystem. *arXiv preprint arXiv:2404.10518*, 2024. 5
- [41] Linhao Qu, Manning Wang, Zhijian Song, et al. Bi-directional weakly supervised knowledge distillation for whole slide image classification. *Advances in Neural Information Processing Systems*, 35:15368–15381, 2022. 1
- [42] Jan Ramon. Multi instance neural networks. In *ML-2000 Workshop Attribute-Value and Relational Learning*, 2000. 2
- [43] Yongming Rao, Wenliang Zhao, Benlin Liu, Jiwen Lu, Jie Zhou, and Cho-Jui Hsieh. Dynamicvit: Efficient vision transformers with dynamic token sparsification. *Advances in neural information processing systems*, 34:13937–13949, 2021. 2, 3, 5
- [44] Joel Saltz, Rajarsi Gupta, Le Hou, Tahsin Kurc, Pankaj Singh, Vu Nguyen, Dimitris Samaras, Kenneth R Shroyer, Tianhao Zhao, Rebecca Batiste, et al. Spatial organization and molecular correlation of tumor-infiltrating lymphocytes using deep learning on pathology images. *Cell reports*, 23(1):181–193, 2018. 1
- [45] Denis Schapiro, Hartland W Jackson, Swetha Raghuraman, Jana R Fischer, Vito RT Zanotelli, Daniel Schulz, Charlotte Giesen, Raúl Catena, Zsuzsanna Varga, and Bernd Bodenmiller. histocat: analysis of cell phenotypes and interactions in multiplex image cytometry data. *Nature methods*, 14(9):873–876, 2017. 1
- [46] Wei Shao, Tongxin Wang, Zhi Huang, Zhi Han, Jie Zhang, and Kun Huang. Weakly supervised deep ordinal cox model for survival prediction from whole-slide pathological images. *IEEE Transactions on Medical Imaging*, 40(12):3739–3747, 2021. 1
- [47] Zhuchen Shao, Hao Bian, Yang Chen, Yifeng Wang, Jian Zhang, Xiangyang Ji, et al. Transmil: Transformer based correlated multiple instance learning for whole slide image classification. *Advances in neural information processing systems*, 34:2136–2147, 2021. 1, 2, 6
- [48] Lin Song, Songyang Zhang, Songtao Liu, Zeming Li, Xuming He, Hongbin Sun, Jian Sun, and Nanning Zheng. Dynamic grained encoder for vision transformers. *Advances in Neural Information Processing Systems*, 34:5770–5783, 2021. 2
- [49] David A Sprecher and Sorin Draghici. Space-filling curves and kolmogorov superposition-based neural networks. *Neural Networks*, 15(1):57–67, 2002. 2

- [50] Hoang-Thang Ta. Bsrbf-kan: A combination of b-splines and radial basic functions in kolmogorov-arnold networks. *arXiv preprint arXiv:2406.11173*, 2024. [2](#)
- [51] Surat Teerapittayanon, Bradley McDanel, and Hsiang-Tsung Kung. Branchynet: Fast inference via early exiting from deep neural networks. In *2016 23rd international conference on pattern recognition (ICPR)*, pages 2464–2469. IEEE, 2016. [2](#)
- [52] Cristian J Vaca-Rubio, Luis Blanco, Roberto Pereira, and Mărius Caus. Kolmogorov-arnold networks (kans) for time series analysis. *arXiv preprint arXiv:2405.08790*, 2024. [2](#)
- [53] Yulin Wang, Rui Huang, Shiji Song, Zeyi Huang, and Gao Huang. Not all images are worth 16x16 words: Dynamic transformers for efficient image recognition. *Advances in neural information processing systems*, 34:11960–11973, 2021. [2](#)
- [54] Anfeng Xu, Biqiao Zhang, Shuyu Kong, Yiteng Huang, Zhaojun Yang, Sangeeta Srivastava, and Ming Sun. Effective integration of kan for keyword spotting. *arXiv preprint arXiv:2409.08605*, 2024. [2](#)
- [55] Jinfeng Xu, Zheyu Chen, Jinze Li, Shuo Yang, Wei Wang, Xiping Hu, and Edith C-H Ngai. Fourierkan-gcf: Fourier kolmogorov-arnold network—an effective and efficient feature transformation for graph collaborative filtering. *arXiv preprint arXiv:2406.01034*, 2024. [2](#)
- [56] Le Yang, Yizeng Han, Xi Chen, Shiji Song, Jifeng Dai, and Gao Huang. Resolution adaptive networks for efficient inference. In *Proceedings of the IEEE/CVF conference on computer vision and pattern recognition*, pages 2369–2378, 2020. [2](#)
- [57] Shu Yang, Yihui Wang, and Hao Chen. Mambamil: Enhancing long sequence modeling with sequence reordering in computational pathology. *arXiv preprint arXiv:2403.06800*, 2024. [1](#), [2](#), [6](#)
- [58] Xingyi Yang and Xinchao Wang. Kolmogorov-arnold transformer. *arXiv preprint arXiv:2409.10594*, 2024. [2](#)
- [59] Jiawen Yao, Xinliang Zhu, Jitendra Jonnagaddala, Nicholas Hawkins, and Junzhou Huang. Whole slide images based cancer survival prediction using attention guided deep multiple instance learning networks. *Medical Image Analysis*, 65: 101789, 2020. [1](#)
- [60] Xiaotian Yu, Haoming Luo, Jiacong Hu, Xiuming Zhang, Yuexuan Wang, Wenjie Liang, Yijun Bei, Mingli Song, and Zunlei Feng. Hundredfold accelerating for pathological images diagnosis and prognosis through self-reform critical region focusing. [2](#)
- [61] Hongrun Zhang, Yanda Meng, Yitian Zhao, Yihong Qiao, Xiaoyun Yang, Sarah E Coupland, and Yalin Zheng. Dtf-dmil: Double-tier feature distillation multiple instance learning for histopathology whole slide image classification. In *Proceedings of the IEEE/CVF Conference on Computer Vision and Pattern Recognition*, pages 18802–18812, 2022. [1](#), [2](#), [6](#)
- [62] Wangbo Zhao, Jiasheng Tang, Yizeng Han, Yibing Song, Kai Wang, Gao Huang, Fan Wang, and Yang You. Dynamic tuning towards parameter and inference efficiency for vit adaptation. *arXiv preprint arXiv:2403.11808*, 2024. [2](#)
- [63] Wentao Zhu, Qi Lou, Yeeleng Scott Vang, and Xiaohui Xie. Deep multi-instance networks with sparse label assignment for whole mammogram classification. In *Medical Image Computing and Computer Assisted Intervention- MICCAI 2017: 20th International Conference, Quebec City, QC, Canada, September 11-13, 2017, Proceedings, Part III 20*, pages 603–611. Springer, 2017. [2](#)